PARL deficiency in mouse causes Complex III defects, coenzyme Q depletion, and Leigh-like syndrome

Marco Spinazzi[a,b,1], Enrico Radaelli[c], Katrien Horré[a,b], Amaia M. Arranz[a,b], Natalia V. Gounko[a,b,d], Patrizia Agostinis[e], Teresa Mendes Maia[f,g,h], Francis Impens[f,g,h], Vanessa Alexandra Morais[i], Guillermo Lopez-Lluch[j,k], Lutgarde Serneels[a,b], Placido Navas[j,k], and Bart De Strooper[a,b,l,1]

[a]VIB Center for Brain and Disease Research, 3000 Leuven, Belgium; [b]Department of Neurosciences, Katholieke Universiteit Leuven, 3000 Leuven, Belgium; [c]Comparative Pathology Core, Department of Pathobiology, School of Veterinary Medicine, University of Pennsylvania, Philadelphia, PA 19104-6051; [d]Electron Microscopy Platform, VIB Bio Imaging Core, 3000 Leuven, Belgium; [e]Cell Death Research & Therapy Laboratory, Department for Cellular and Molecular Medicine, Katholieke Universiteit Leuven, 3000 Leuven, Belgium; [f]VIB Center for Medical Biotechnology, VIB, 9000 Ghent, Belgium; [g]VIB Proteomics Core, VIB, 9000 Ghent, Belgium; [h]Department for Biomolecular Medicine, Ghent University, 9000 Ghent, Belgium; [i]Instituto de Medicina Molecular, Faculdade de Medicina, Universidade de Lisboa, 1649-028 Lisbon, Portugal; [j]Centro Andaluz de Biología del Desarrollo, Universidad Pablo de Olavide-Consejo Superior de Investigaciones Científicas-Junta de Andalucía, 41013 Seville, Spain; [k]Centro de Investigaciones Biomédicas en Red de Enfermedades Raras, Instituto de Salud Carlos III, 28029 Madrid, Spain; and [l]UK Dementia Research Institute, University College London, WC1E 6BT London, United Kingdom

Edited by Richard D. Palmiter, University of Washington, Seattle, WA, and approved November 21, 2018 (received for review July 11, 2018)

The mitochondrial intramembrane rhomboid protease PARL has been implicated in diverse functions in vitro, but its physiological role in vivo remains unclear. Here we show that *Parl* ablation in mouse causes a necrotizing encephalomyelopathy similar to Leigh syndrome, a mitochondrial disease characterized by disrupted energy production. Mice with conditional PARL deficiency in the nervous system, but not in muscle, develop a similar phenotype as germline *Parl* KOs, demonstrating the vital role of PARL in neurological homeostasis. Genetic modification of two major PARL substrates, PINK1 and PGAM5, do not modify this severe neurological phenotype. *Parl*$^{-/-}$ brain mitochondria are affected by progressive ultrastructural changes and by defects in Complex III (CIII) activity, coenzyme Q (CoQ) biosynthesis, and mitochondrial calcium metabolism. PARL is necessary for the stable expression of TTC19, which is required for CIII activity, and of COQ4, which is essential in CoQ biosynthesis. Thus, PARL plays a previously overlooked constitutive role in the maintenance of the respiratory chain in the nervous system, and its deficiency causes progressive mitochondrial dysfunction and structural abnormalities leading to neuronal necrosis and Leigh-like syndrome.

rhomboid protease | mitochondria | neurodegeneration | respiratory chain | Leigh syndrome

PARL represents the only known mitochondrial member of the rhomboid family (1). Rhomboids are evolutionary conserved intramembrane cleaving proteases and pseudoproteases involved in a variety of functions (2). Their broad biological significance is reflected in their pathological relevance for prevalent human diseases, including cancer and neurodegenerative diseases (2).

The crucial role of PARL in cellular homeostasis is illustrated by the lethal multisystem phenotype of PARL-deficient (*Parl*$^{-/-}$) mice, associated with muscle atrophy and increased apoptosis in thymus and spleen (3). The faster cytochrome *c* release and cristae remodeling in vitro, and the increased cell death of *Parl*$^{-/-}$ mouse embryonic fibroblasts (MEFs) treated with apoptosis-inducing agents rescued by overexpressed intermembrane space-targeted OPA1, led to the proposal that PARL plays a role in cristae remodeling and cytochrome *c* release during apoptosis. The authors suggested that decreased OPA1 processing by PARL was causative of these apoptotic phenotypes. Later studies identified OMA1 and YME1L (4) as the proteases cleaving OPA1 and questioned OPA1 as a PARL substrate. More recently, PARL has been implicated in the processing of other substrates in cultured cells (5–10). Two substrates, PINK1 and PGAM5, are of particular interest because they are implicated in Parkinson's disease (11, 12). Both accumulate in *Parl*$^{-/-}$ cells (6–9, 13), but it is unclear whether this accumulation is detrimental (1). A recent elegant cell-biology study proposed that PARL exerts proapoptotic effects via misprocessing of the mitochondrial Diablo homolog (hereafter DIABLO) (10). However, this is difficult to reconcile with the lethality of *Parl*$^{-/-}$ mice and the proposed protective function of PARL (3). Overall, the available data have led to contradictory speculations with regard to the role of PARL in apoptosis (3, 10), mitochondrial function (3, 14), morphology (3, 14, 15), and mitophagy (16–18), and claims have not been further substantiated in vivo. More importantly, the cause of death of the *Parl*$^{-/-}$ mice, and therefore the physiological role of this protease, has remained unresolved. To address these questions, we reinvestigated PARL-deficient mice. In contrast with our previous report, we find now that, in addition to the described phenotypes in peripheral tissues, PARL deficiency causes a necrotizing encephalomyelopathy closely resembling Leigh syndrome, a human mitochondrial disease caused by impaired energy metabolism (19). A similar multisystem phenotype is seen in the full *Parl*$^{-/-}$ and in *Parl*$^{L/L}$::*Nes*^{Cre} mice with a specific deletion of PARL in the nervous system. The striking neurodegeneration is not associated with altered apoptosis but with massive necrosis, raising

Significance

PARL is a peculiar protease in the inner membrane of mitochondria with important but unclear physiological roles and with links to Parkinson's disease and diabetes. Most studies, including the original characterization of the *Parl*-KO mouse and others performed in vitro, have focused on apoptosis. Here we show that PARL deficiency in the nervous system alone or in the complete animal causes severe neurodegeneration associated with necrosis resembling the human mitochondrial disease Leigh syndrome. By combining genetic, biochemical, and proteomic approaches, we show that PARL plays an essential physiological role in the nervous system being required for the maintenance of mitochondrial structure and function at the level of Complex III, coenzyme Q, and calcium metabolism.

Author contributions: M.S., L.S., P.N., and B.D.S. designed research; M.S., E.R., K.H., A.M.A., N.V.G., F.I., V.A.M., and G.L.-L. performed research; P.A. contributed new reagents/analytic tools; M.S., E.R., K.H., A.M.A., T.M.M., F.I., G.L.-L., L.S., P.N., and B.D.S. analyzed data; M.S. and B.D.S. wrote the paper; and P.A. provided critical feedback.

The authors declare no conflict of interest.

This article is a PNAS Direct Submission.

Data deposition: The MS proteomics data have been deposited to the ProteomeXchange Consortium via the PRIDE partner repository with the dataset identifier PXD008908.

[1]To whom correspondence may be addressed. Email: maspinazzi@gmail.com or bartdestrooper@kuleuven.vib.be.

This article contains supporting information online at www.pnas.org/lookup/suppl/doi:10.1073/pnas.1811938116/-/DCSupplemental.

Published online December 21, 2018.

the question of the underlying mechanism. We show that necrosis in *Parl*$^{-/-}$ brains is preceded by progressive mitochondrial structural changes and by early respiratory chain defects at the level of Complex III (CIII) and coenzyme Q (CoQ), and is associated with altered mitochondrial calcium metabolism. Thus, PARL has an essential physiological role in the maintenance of mitochondrial structure and function, which is severely impaired when PARL is ablated, causing Leigh-like neurodegeneration. We discuss how these insights affect our previous interpretations of the *Parl*$^{-/-}$ phenotype in vivo.

Results

PARL Deficiency in the Nervous System Leads to a Severe Encephalomyelopathy Resembling Leigh Syndrome. *Parl*$^{-/-}$ mice develop normally up to the age of 40 d, after which they progressively lose weight (3). From the age of 6 wk, they show rapidly progressive locomotor impairment, paresis of the lower limbs, hunched back, and dyspnea (Movie S1). They die before the age of 8 wk with a multisystem phenotype with atrophic muscles, thymus, and spleen (3), without a clear explanation. Immune deficiency is unlikely the cause of death because thymus and spleen atrophy only a few days before death, when mice are already severely affected. Moreover, mice are bred in specific pathogen-free conditions and do not develop opportunistic infections, leaving open the question of which essential vital function is compromised by PARL deficiency. These clinical signs led us to ask whether this phenotype was caused by neurological involvement. Examination of the brain and spinal cord from *Parl*$^{-/-}$ mice indeed showed a previously overlooked subcortical vacuolar encephalomyelopathy closely resembling Leigh syndrome (Fig. 1 *A*–*H*). Leigh syndrome is a lethal mitochondrial disease characterized by neurological regression and pathologically by vacuolar degeneration and necrosis of the brainstem, basal ganglia, and spinal cord; reactive gliosis; and vascular proliferation (20). Vacuolization of the neuropil was first detectable in *Parl*$^{-/-}$ mice at 5 wk of age, initially circumscribed in the brainstem and in the gray matter of the spinal cord, and then progressively extending anteriorly to hypothalamus, thalamus, deep cerebellar nuclei, and the cingulate cortex. Other areas of the brain, notably most of the cortex, hippocampus, and substantia nigra, were spared. Neuronal loss was detectable by loss of RBFOX3 (NEUN)-positive cells (Fig. 1*B*). Neurodegeneration was accompanied by extensive astrogliosis and microgliosis, indicated by GFAP (Fig. 1*C*) and IBA1 immunoreactivity (Fig. 1*D*). Luxol fast blue, a stain used to visualize the white matter, showed comparable reaction in WT and *Parl*$^{-/-}$ mice (Fig. 1*E*). Consistent with neuronal involvement, in situ hybridization shows that *Parl* mRNA expression was particularly abundant in neurons (Fig. 1*F*). In advanced stages, vascular proliferation became evident (Fig. 1*G*), and symmetrical hemorrhages were frequently observed at 7 wk of age in the most severely affected areas of the brainstem and spinal cord (Fig. 1*H*). When *Parl* was specifically ablated in the nervous system by using a Nestin-Cre driver (*Parl*$^{L/L}$::*Nes*^{Cre}; Fig. 1*J*), a similar lethal phenotype was observed as in the germline *Parl*$^{-/-}$ mice (Fig. 1*I*), including the Leigh-like neuropathology (Fig. 1*K*). Apart from a 4-wk delay in lethality and the absent testis atrophy (Fig. 1*O*), these mice developed the typical *Parl*$^{-/-}$ multisystem phenotype (3) with severe atrophy of muscle, liver, spleen (Fig. 1 *L*–*N*), and thymus (Fig. 1*P*) despite normal PARL expression in these tissues (Fig. 1*J*). To further assess ectopic Cre-mediated recombination in these peripheral tissues, we evaluated the presence of recombination by PCR, followed by high-resolution capillary electrophoresis (*SI Appendix*, Fig. S1 *A* and *B*). *Parl*$^{-/-}$ alleles were nondetectable in *Parl*$^{L/L}$::*Nes*^{Cre} spleen and liver and were present in a very low percentage in thymus (2%) and muscle (5%), consistent with the protein data. Thymus and spleen became atrophic in *Parl*$^{L/L}$::*Nes*^{Cre}, as in germline *Parl*$^{-/-}$ mice, only in preterminal stages of the disease, when the mice were already affected by severe neurological deficits. Conversely, deletion of PARL in striated muscle in *Parl*$^{L/L}$::*Ckmm*^{Cre} KO mice using *Cre* expression driven by the creatine kinase promoter did not compromise survival, at least up to the age of 18 mo, nor did it lead to overt locomotor deficits (n = 13; Fig. 1*I*). Altogether, these data suggest that PARL deficiency in the nervous system is sufficient to recapitulate the lethal multisystem phenotype of germline *Parl*$^{-/-}$ mice, except for the gonad atrophy.

PARL Deficiency Causes Early Neuronal Mitochondrial Ultrastructural Abnormalities Followed by Neuronal Necrosis. To characterize mitochondrial ultrastructure and the morphological features of cell death induced by PARL deficiency in the brain, we performed EM. At 3 wk of age, which is before the occurrence of clinical signs or histopathological lesions, *Parl*$^{-/-}$ but not WT neurons of medulla oblongata displayed scattered swollen mitochondria with abnormal cristae and a translucent matrix (Fig. 2*A*). At later time points, mitochondrial ultrastructural abnormalities became progressively more severe and diffuse in the context of progressive neuronal vacuolization, swelling, and loss of integrity (Fig. 2 *B* and *C*). This picture is indicative of necrosis, and the typical morphological signs of apoptosis were consistently absent. Similar abnormalities were present in neuronal mitochondria from *Parl*$^{L/L}$::*Nes*^{Cre} mice (*SI Appendix*, Fig. S2). As PARL has been linked previously to apoptosis (3, 10), we further investigated its contribution to the neurodegeneration. During apoptosis, the outer mitochondrial membrane becomes permeable, and cytochrome *c* is released from the mitochondrial intermembrane space to the cytosol, leading to proteolytic activation of executioner caspases and PARP1. We analyzed mitochondrial outer membrane permeability of brain mitochondria isolated from symptomatic *Parl*$^{-/-}$ mice by measuring the enhancement of Complex IV (CIV)-driven respiration before and after addition of exogenous cytochrome *c*, which is unable to reach CIV if outer membranes are intact. Cytochrome *c* did not significantly enhance CIV-driven respiration in WT and *Parl*$^{-/-}$ brain mitochondria (Fig. 2*D*), indicating intact outer mitochondrial membranes despite being isolated at an age when *Parl*$^{-/-}$ brains are already affected by significant neurodegeneration. Consistently, cytochrome *c* was undetectable in purified brain cytosols from *Parl*$^{-/-}$ brains (Fig. 2*E*), and the expression of full-length PARP1 was similar in *Parl*$^{-/-}$ and WT brains without evidence of proteolytic activation (Fig. 2*F*). Accordingly, we did not see TUNEL-positive cells in the degenerating brain areas, notably the brainstem, thalamus, and hypothalamus, at serial time points ranging from asymptomatic to late stage of the disease (*SI Appendix*, Fig. S3*A*). TUNEL positivity was restricted to a few scattered cells undergoing developmental apoptosis in periventricular areas such as the hippocampus that were not affected by *Parl*$^{-/-}$ neurodegeneration. This was not more severe in *Parl*$^{-/-}$ than in WT brains. We obtained similar results by using antibodies against cleaved CASP3 in *Parl*$^{-/-}$ (Fig. 2 *G* and *H*) and in *Parl*$^{L/L}$::*Nes*^{Cre} mice (*SI Appendix*, Fig. S3*B*), indicating that apoptosis is not overtly altered in PARL-deficient brains. Conversely, cleaved CASP3 immunostaining of atrophic thymus of severely affected *Parl*$^{-/-}$ mice showed strong positivity (*SI Appendix*, Fig. S3*C*) as previously reported (3). However, an identical thymus pathology (Fig. 1*P*) and CASP3 positivity (*SI Appendix*, Fig. S3*C*) were also seen in late-stage *Parl*$^{L/L}$::*Nes*^{Cre} mice despite normal PARL expression in this tissue (Fig. 1*J*), indicating that this phenotype can be fully induced by deficiency of PARL in the nervous system alone. Treatment of primary cultures of *Parl*$^{-/-}$ and WT neurons with the proapoptotic drug etoposide showed similar proteolytic activation of CASP3 and PARP1, indicating that apoptosis execution is not overtly blocked in cultured neurons either (Fig. 2*I*). All together, these data indicate that the striking neurodegeneration induced by PARL deficiency is preceded by

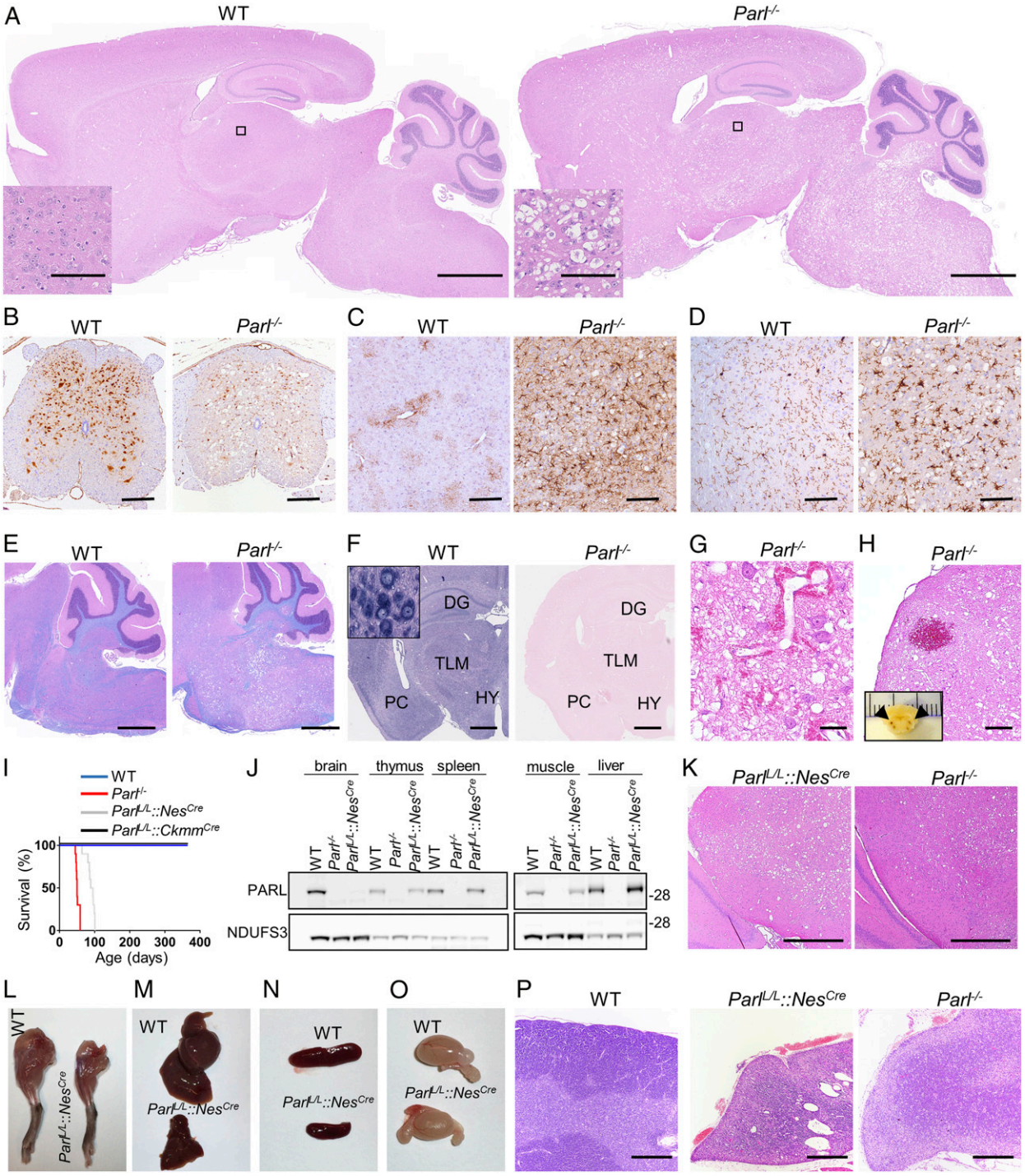

Fig. 1. A Leigh-like encephalomyelopathy drives $Parl^{-/-}$ phenotype. (*A*) Severe vacuolar neurodegeneration in a 7-wk-old $Parl^{-/-}$ mouse brain (H&E staining; $n \geq 12$). (Scale bar: 1,250 μm.) (*Inset*) Detail of the thalamus. (Scale bars: 100 μm.) (*B*) Severe neuronal loss in the gray matter of $Parl^{-/-}$ lumbar spinal cord at 7 wk of age (RBFOX3 staining; $n = 3$ for WT, $n = 6$ for $Parl^{-/-}$). (Scale bar: 125 μm.) (*C*) GFAP staining showing prominent astrogliosis in $Parl^{-/-}$ medulla oblongata at 7 wk of age ($n = 3$ for WT, $n = 6$ for $Parl^{-/-}$). (Scale bar: 125 μm.) (*D*) IBA1 staining in superior colliculus of the midbrain at 7 wk ($n = 3$ for WT, $n = 6$ for $Parl^{-/-}$). (Scale bar: 125 μm.) (*E*) Combined Luxol fast blue and H&E staining show preservation of the white matter (stained in blue) in 7-wk-old $Parl^{-/-}$ mice ($n = 3$ for WT, $n = 7$ for $Parl^{-/-}$). (Scale bar: 750 μm.) (*F*) *Parl* in situ hybridization. DG, dentate gyrus; HY, hypothalamus; PC, pyriform cortex; TLM, thalamus. (Scale bar: 1 mm.) (*Inset*) Strong *Parl* expression in WT reticular neurons (magnification: 100×). (*G*) H&E stain of the inferior colliculus in the midbrain of a 7-wk-old $Parl^{-/-}$ mouse showing vascular proliferation ($n > 10$). (Scale bar: 50 μm.) (*H*) Focal hemorrhage in the olivary nucleus of a 7-wk-old $Parl^{-/-}$ mouse. Bilateral symmetrical hemorrhages have been detected in brainstems of four of seven $Parl^{-/-}$ mice at 7 wk of age and in none of the WT littermates. (Scale bar: 250 μm.) (*Inset*) Bilateral symmetrical hemorrhages in medulla oblongata (arrows). (*I*) Survival curves of WT ($n = 14$), $Parl^{-/-}$ ($n = 14$), $Parl^{L/L}$::Nes^{Cre} ($n = 15$), and $Parl^{L/L}$::$Ckmm^{Cre}$ mice ($n = 13$). (*J*) Western blot analysis of PARL protein in brain, thymus, spleen, muscle, and liver mitochondria isolated from 7-wk-old WT and $Parl^{-/-}$ and 13-wk-old $Parl^{L/L}$::Nes^{Cre} mice ($n = 3$). NDUFS3 is the loading control. (*K*) H&E stain of midbrains from 10-wk-old $Parl^{L/L}$::Nes^{Cre} ($n = 4$) and 7-wk-old $Parl^{-/-}$ mice ($n = 12$). (Scale bar: 380 μm.) (*L–O*) Severe atrophy of the skeletal muscle (*L*), liver (*M*), and spleen (*N*) but normal testis size (*O*) are seen in 11-wk-old $Parl^{L/L}$::Nes^{Cre} male mice compared with an age-matched WT control ($n > 15$). (*P*) H&E stain of thymus from WT (age 7 wk; $n = 6$), $Parl^{L/L}$::Nes^{Cre} (age 10–13 wk; $n = 4$), and $Parl^{-/-}$ mice (age 7 wk; $n = 12$). $Parl^{L/L}$::Nes^{Cre} and $Parl^{-/-}$ thymus are atrophic. (Scale bar: 200 μm.)

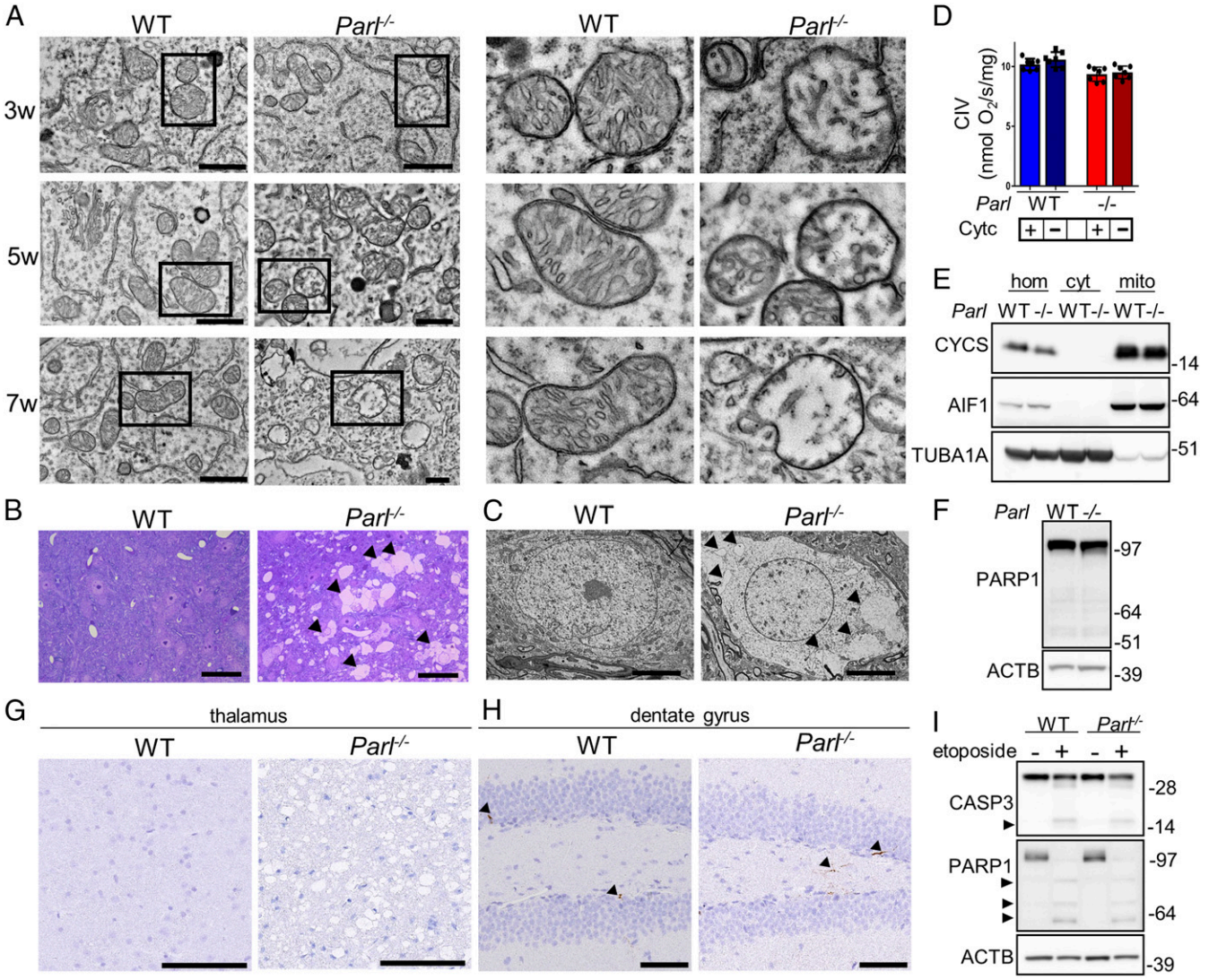

Fig. 2. *Parl*$^{-/-}$ neurodegeneration is preceded by mitochondrial structural changes and is characterized by necrosis. (*A*) EM images of medulla oblongata neuronal mitochondria of WT and *Parl*$^{-/-}$ over time at 3, 5, and 7 wk of age. (*Right*) High-magnification inset of images at left. (Scale bar: 1 μm.) (*B*) Semithin section stained with toluidine blue shows vacuolization and disintegration of neurons (black arrowheads) in medulla oblongata of 7-wk-old *Parl*$^{-/-}$ mouse compared with WT. (Scale bar: 50 μm.) (*C*) Representative EM images showing intracellular vacuolization (black arrowheads) in a 7-wk-old *Parl*$^{-/-}$ thalamic neuron. (Scale bar: 5 μm.) (*D*) Permeability of mitochondrial outer membrane by ascorbate/TMPD-driven oxygen consumption rates in 6-wk-old WT and *Parl*$^{-/-}$ purified free brain mitochondria ($n = 7$) before and after addition of 10 μM cytochrome *c*. Data represent average ± SD. (*E*) Western blot of WT and *Parl*$^{-/-}$ brain cytosolic and mitochondrial fractions at 7 wk of age ($n = 3$) showing absent cytochrome *c* in the cytosol. Anti-AIF1 and anti-TUBA1A are the mitochondrial and cytosolic markers. cyt, purified cytosol; Hom, total homogenate; mito, purified mitochondria. (*F*) Immunoblot of 7-wk-old WT and *Parl*$^{-/-}$ brain nuclei-enriched fractions with anti-PARP1 antibody. (*G*) Activated CASP3 staining shows absence of positive neurons in 7-wk *Parl*$^{-/-}$ thalamus despite severe neurodegeneration ($n = 4$). (Scale bar: 100 μm.) (*H*) In the dentate gyrus, a brain area that does not degenerate in germline or in *Parl*$^{L/L}$::*Nes*^{Cre} mice, activated CASP3 staining shows scattered positive neurons (black arrows) to the same extent in WT and *Parl*$^{-/-}$ mice ($n = 4$). (Scale bar: 50 μm.) (*I*) Cultured primary neurons were treated with 10 μM etoposide for 24 h and lysed. Total neuronal lysates were immunoblotted with anti-CASP3 and anti-PARP1 antibodies. The black arrows indicate the proteolyzed CASP3 and PARP1. ACTB is the loading control.

mitochondrial ultrastructural abnormalities that accumulate over time. The neurodegeneration is characterized by neuronal necrosis without overtly altered apoptosis. The increased apoptosis in *Parl*$^{-/-}$ immune organs is indirect.

***Parl*$^{-/-}$ Leigh-Like Encephalomyelopathy Is Not Caused by Misprocessing of PINK1 and PGAM5.** Next, we wondered to what extent the neurodegeneration of *Parl*$^{-/-}$ mice can be attributed to misprocessing of the best characterized substrates of PARL, PINK1 (6, 8, 16), a mitochondrial kinase, and PGAM5, a mitochondrial phosphatase (9). Both have roles in neurological diseases (11, 12) and in mitophagy (12, 21). PGAM5 has also been linked to regulation of multiple cell death pathways including necroptosis (22). However, the contribution of PINK1 and PGAM5 misprocessing to the *Parl*$^{-/-}$ phenotype is not known (1). Expression of LC3, SQSTM1, and BNIP3 (*SI Appendix*, Fig. S4*A*), which are markers of macroautophagy, and mitochondrial protein ubiquitination (*SI Appendix*, Fig. S4*B*), which labels proteins of dysfunctional mitochondrial for degradation by mitophagy, were not modified in *Parl*$^{-/-}$ brains, indicating unaltered steady-state autophagy in *Parl*$^{-/-}$ brain. PINK1 was barely detectable in WT mitochondria, whereas a remarkable accumulation of PINK1 was seen in *Parl*$^{-/-}$ brain mitochondria (Fig. 3*A*). Similarly, the unprocessed full-length form of PGAM5 strongly accumulated in *Parl*$^{-/-}$ mitochondria whereas the processed form of PGAM5

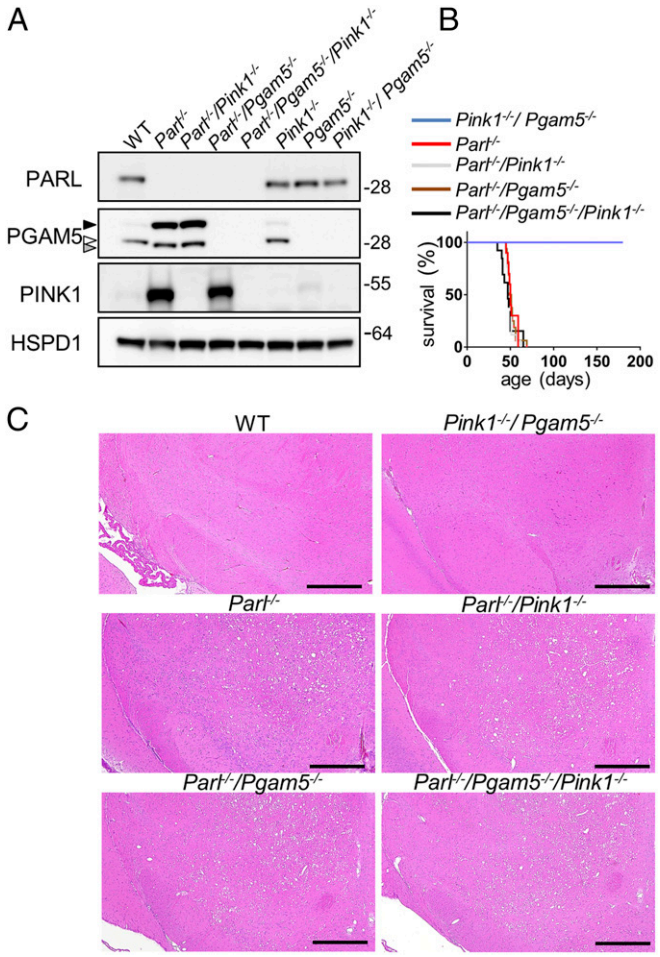

Fig. 3. *Pink1* and *Pgam5* do not interact genetically with *Parl* deficiency in vivo. (*A*) Validation of $Parl^{-/-}/Pgam5^{-/-}$, $Parl^{-/-}/Pink1^{-/-}$, and $Pink1^{-/-}/Pgam5^{-/-}$ double-KO mice and $Parl^{-/-}/Pgam5^{-/-}/Pink1^{-/-}$ triple-KO mice. Brain mitochondria were isolated from mice of the indicated genotype and immunoblotted with PARL, PINK1, and PGAM5 antibodies. The white arrow indicates the mature form of PGAM5, the black arrow indicates the unprocessed form, and the gray arrow indicates alternatively processed form in $Parl^{-/-}$ mitochondria. HSPD1 is the loading control. (*B*) Survival curves of $Parl^{-/-}$ ($n = 10$), $Pink1^{-/-}/Pgam5^{-/-}$ ($n = 10$), $Parl^{-/-}/Pink1^{-/-}$ ($n = 17$), $Parl^{-/-}/Pgam5^{-/-}$ ($n = 16$), and $Parl^{-/-}/Pgam5^{-/-}/Pink1^{-/-}$ ($n = 13$). (*C*) H&E staining of midbrain coronal sections of 7-wk-old mice of the indicated genotypes ($n > 3$). (Scale bar: 500 μm.)

migrated slightly faster than in WT mitochondria, indicating an alternative PARL-independent cleavage. To test whether accumulation of these unprocessed forms of PINK1 and PGAM5 in $Parl^{-/-}$ mitochondria drives $Parl^{-/-}$ neurodegeneration, we generated a series of double $Parl^{-/-}/Pink1^{-/-}$, $Parl^{-/-}/Pgam5^{-/-}$ and triple $Parl^{-/-}/Pink1^{-/-}/Pgam5^{-/-}$ combined KO mice (Fig.3*A*). Surprisingly, the $Parl^{-/-}$ phenotype was unmodified by simultaneous deletion of PINK1 or PGAM5 alone or together, and all these mouse strains invariably died at a similar age as the single $Parl^{-/-}$ mice (Fig. 3*B*) affected by similar Leigh-like syndrome (Fig. 3*C*). To test whether deficient proteolytic products of PINK1 and PGAM5 generated by PARL were essential, we also generated $Pink1^{-/-}/Pgam5^{-/-}$ mice. Conversely, $Pink1^{-/-}/Pgam5^{-/-}$ mice had a normal lifespan (Fig. 3*B*) beyond the age of 2 y without any overt clinical or neuropathological phenotype (Fig. 3*C*), indicating that misprocessing of PINK1 and PGAM5 alone or together do not explain the $Parl^{-/-}$-associated Leigh-like syndrome.

PARL Deficiency Leads to Severe Respiratory Chain Defects Converging on CIII and CoQ. Leigh syndrome is caused by different genetic defects that ultimately impair mitochondrial energy production, most commonly by affecting the respiratory chain (19). Therefore, we evaluated how brain mitochondrial function is compromised by absent PARL expression. As PARL has been previously linked to differences in mitochondrial biogenesis (14), we asked whether mitochondrial mass is affected in $Parl^{-/-}$ brains. Expression of respiratory chain subunits and of the outer membrane protein TOMM20 was similar in WT and $Parl^{-/-}$ brains at any age (Fig. 4*A*), indicating unaltered mitochondrial mass. Mitochondrial DNA abundance was also not significantly different (Fig. 4*F*). Next, we measured oxygen consumption rates by high-resolution respirometry in neuronal mitochondria derived from permeabilized synaptosomes supplied consecutively with substrates and specific inhibitors for Complex I (CI), Complex II (CII), and CIV as illustrated in Fig. 4*B*. Importantly, at 3 wk of age, which is 3 wk before the first clinical signs in $Parl^{-/-}$ mice, respiration was comparable between WT and $Parl^{-/-}$ brain mitochondria (*SI Appendix*, Fig. S5*A*). However, at 6 wk of age, at the onset of the symptomatic stage, ADP-stimulated respiration [i.e., oxidative phosphorylation (OXPHOS)], reflecting the maximal capacity to generate ATP, and uncoupled respiration, providing an estimate of the maximal electron transfer (ET) capacity, were severely diminished in $Parl^{-/-}$ neuronal mitochondria (Fig. 4*C*). Oxygen consumption was similarly decreased when using only CI substrates (i.e., CI OXPHOS) or CI and CII substrates simultaneously in phosphorylating and uncoupled states (i.e., CI+CII OXPHOS and ET). Respiration from cytochrome *c* oxidase (i.e., CIV) was slightly, although significantly, compromised (Fig. 4*C*). To localize precisely the respiratory chain defect, we measured the maximal enzymatic activities of each complex (i.e., CI–CV) in brain mitochondria, as well as the coupled enzymatic activity of CII plus CIII. This latter enzymatic assay explores segment CII–CoQ–CIII. We detected a severe enzymatic defect of CIII and of CII plus CIII (Fig. 4*D*), whereas CII and CIV activities were slightly, although still significantly, decreased. Next, we wondered whether the deficient CIII activity was caused by abnormal CIII assembly. Blue native gel electrophoresis of brain mitochondria showed effective assembly and maturation of the four respiratory chains CI–CIV and of ATP synthase, as well as preserved formation of the super complex (Fig. 4*E*). The terminal component of CIII, UQCRFS1, was normally incorporated, but $CIII_2$ consistently showed a slightly lower electrophoretic mobility in $Parl^{-/-}$ compared with WT mitochondria (Fig. 4*E*). An identical $CIII_2$ migration abnormality has been recently reported in mitochondria deficient of TTC19 (23), and gene mutations in *TTC19* cause human Leigh syndrome (24). Next, to investigate unambiguously the possibility of CoQ deficiency, we directly measured CoQ levels (CoQ_{9+10}) in brain extracts and the ratio between reduced and oxidized CoQ, a sensitive marker of the ET efficiency (25). CoQ deficiency is one of the established causes of Leigh syndrome (19). Remarkably, total CoQ levels were severely decreased in $Parl^{-/-}$ brains at 7 wk of age (Fig. 4*G*). Moreover, the ratio between reduced and oxidized forms of CoQ was strongly increased (Fig. 4*H*), indicating a marked impairment in $CoQH_2$ oxidation, consistent with the impaired CIII activity. These changes were in contrast to the respiration defect, already severe at the presymptomatic age of 3 wk (*SI Appendix*, Fig. S5*B*), indicating that CoQ deficiency is an early effect of PARL deficiency. In conclusion, PARL is required to prevent severe alterations in the respiratory chain of brain mitochondria characterized by CIII and CoQ biosynthesis defects.

Altered Calcium Metabolism, Membrane Potential, and Reactive Oxygen Species Production in $Parl^{-/-}$ Brain Mitochondria. Next, we wondered whether PARL deficiency compromises other important mitochondrial functions in brain mitochondria. Increased

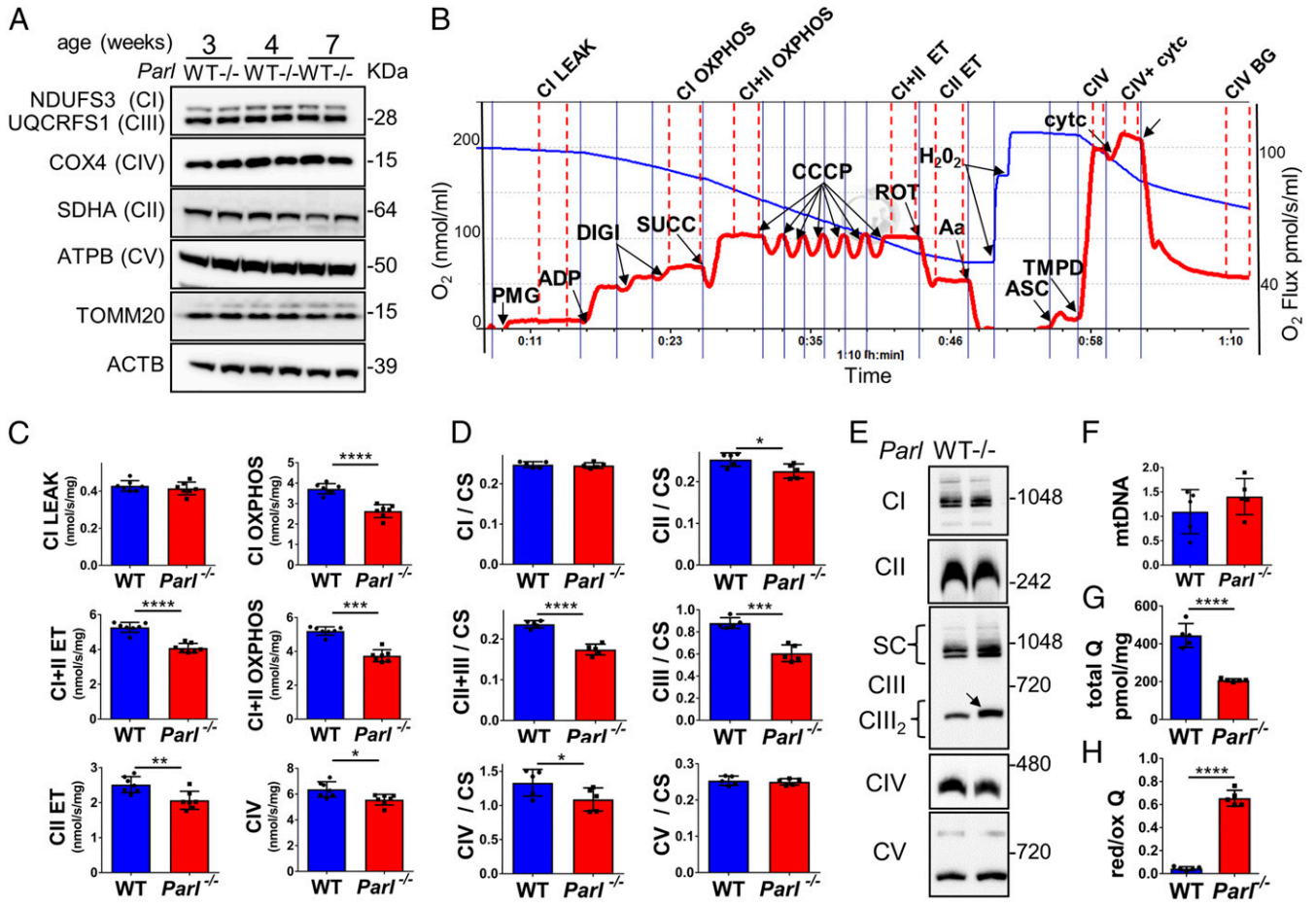

Fig. 4. Defects in CIII and CoQ in *Parl*$^{-/-}$ brain mitochondria. (*A*) Immunoblot of respiratory chain subunits (CI–CV), TOMM20, in WT and *Parl*$^{-/-}$ whole brain lysates at 3, 4, and 7 wk of age ($n = 4$). ACTB is the loading control. (*B*) Representative trace illustrating the protocol for high-resolution respirometry in neuronal mitochondria. The blue trace indicates the O_2 concentration and the red trace indicates its time derivative. Purified synaptosomes (50 μg) were loaded in Miro6 buffer. Digitonin (Digi) was titrated to achieve optimal synaptosomal permeabilization. Substrates are as follows: CI (PMG, pyruvate + malate + glutamate), CII (Succ, succinate), and CIV (ASC/TMPD, ascorbate + TMPD). The uncoupler is CCCP. Inhibitors are as follows: CI (ROT, rotenone), CIII (Aa, Antimycin a), and CIV (KCN, potassium cyanide). Respiratory states are indicated between red dashed lines. CI LEAK, CI-driven leak respiration; CI OXPHOS, CI-driven phosphorylating respiration; CI+II OXPHOS, phosphorylating respiration driven by combined activation of CI and II; CI+II ET, electron transfer capacity driven by combined CI and II; CII ET, ET driven by CII; CIV, CIV-driven respiration; Cytc, exogenous cytochrome *c* is added to evaluate the integrity of the outer mitochondrial membranes. H_2O_2 in the presence of catalase is used to reoxygenate the chamber. (*C*) Quantification of the respiratory states of permeabilized synaptosomes isolated from 6-wk-old WT and *Parl*$^{-/-}$ mice ($n = 7$) as from the protocol in *B*. (*D*) Enzymatic activities of individual respiratory chain complexes and CII+CIII in brain mitochondria from 6-wk-old WT and *Parl*$^{-/-}$ mice ($n = 5$) normalized to citrate synthase. (*E*) Blue native gel electrophoresis of purified brain mitochondria from 7-wk-old WT and *Parl*$^{-/-}$ mice, followed by immunoblotting with anti-NDUFS3 (CI), anti-SDHA (CII), anti-UQCRFS1 (CIII), anti-COX4I1 (CIV), and anti-ATP5B (CV). The arrow indicates the upward mobility change of $CIII_2$ in *Parl*$^{-/-}$ ($n = 3$). (*F*) Mitochondrial DNA normalized by nuclear DNA in 7-wk-old WT and *Parl*$^{-/-}$ brainstems ($n = 5$). (*G*) Concentration of total CoQ (Q_9+Q_{10}) measured by HPLC in brain tissue from 7-wk-old WT and *Parl*$^{-/-}$ mice ($n = 5$). (*H*) CoQ red/ox ratio from the experiment in *G*. Bar graphs indicate average ± SD. Statistical significance calculated by two-sided Student *t* test: $^{*}P < 0.05$, $^{**}P < 0.01$, $^{***}P < 0.001$, and $^{****}P < 0.0001$.

production of reactive oxygen species (ROS) can follow respiratory chain defects. Therefore, we measured ROS production rates in brain mitochondria supplemented with CI and CII substrates by fluorimetry with the H_2O_2 sensor Amplex UltraRed as illustrated in *SI Appendix*, Fig. S6*A*. ROS production was similar in all experimental conditions except for a slight increase only with CI substrates (*SI Appendix*, Fig. S6*B*). Consistently, protein carbonylation, a commonly used biomarker to assess oxidative stress ex vivo, was not increased in *Parl*$^{-/-}$ brain mitochondria or total homogenates compared with WT (*SI Appendix*, Fig. S6 *C* and *D*).

Mitochondrial calcium is an important determinant of cell death and is bidirectionally related to energy metabolism. Excessive levels of mitochondrial calcium and reduced buffering of cytosolic calcium can be detrimental (26). Therefore, we measured the maximal calcium retention capacity in purified brain mitochondria progressively loaded with calcium (Fig. 5*A*, *Left*). *Parl*$^{-/-}$ brain mitochondria showed a severely reduced calcium capacity (Fig. 5*A*, *Right*). To investigate whether this defect could be explained by mitochondrial depolarization, we measured the mitochondrial potential ($\Delta\psi$) in brain mitochondria supplied with CI and CII substrates in the absence and presence of ADP (Fig. 5*B*). In this experiment, $\Delta\psi$ is inversely related to the fluorescence of safranin, which is quenched in the mitochondrial matrix of polarized mitochondria. As expected, the addition of ADP consistently led to increased fluorescence, corresponding to a decrease in $\Delta\psi$ which reflects the use of the proton gradient to drive ATP synthesis, and the mitochondrial uncoupler CCCP led to a further increase. $\Delta\psi$ in *Parl*$^{-/-}$ brain mitochondria was diminished only in the presence of ADP (in phosphorylating conditions) with the use of both CI and CII substrates (Fig. 5 *C* and *D*, *Right*), whereas the maximal $\Delta\psi$ measured in the absence

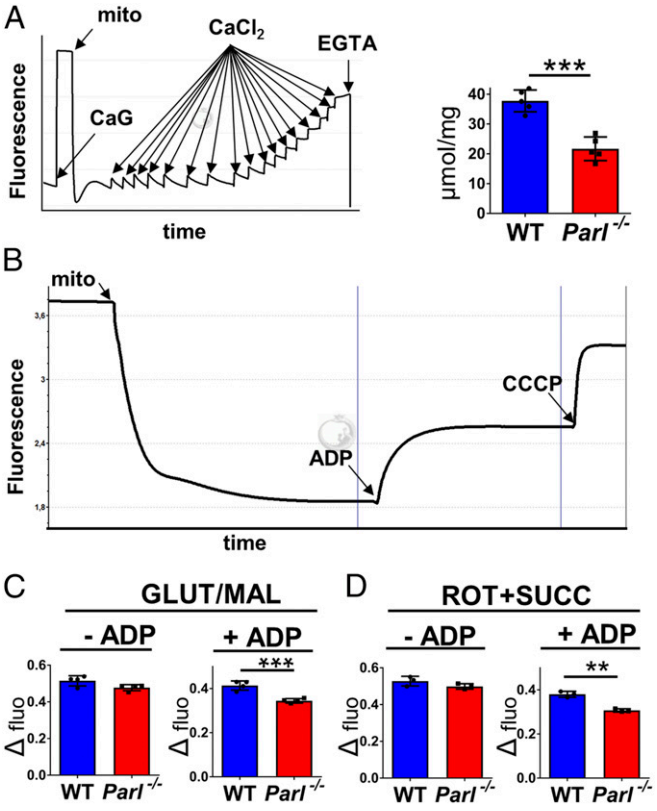

Fig. 5. Alterations in calcium uptake and membrane potential in *Parl*$^{-/-}$ brain mitochondria. (*A*) Calcium-retaining capacity of purified brain mitochondria. (*Left*) Representative trace of a typical fluorimetric experiment using Calcium Green illustrates the protocol detailed in *SI Appendix, Material and Methods*. $CaCl_2$, calcium chloride titrations; CaG, Calcium Green; EGTA, calcium chelator; Mito, mitochondria. (*Right*) Graph bars represent the quantifications of the maximal amount of exogenous calcium retained by WT and *Parl*$^{-/-}$ brain mitochondria purified from 6-wk-old mice before observing calcium efflux ($n = 5$). (*B*) Mitochondrial membrane potential (i.e., $\Delta\psi$) in brain mitochondria using safranin. A typical fluorimetric experiment illustrates the protocol detailed in *SI Appendix, Material and Methods*. CCCP is the uncoupler. Mito, mitochondria. (*C* and *D*) Quantifications of the experiments described in *A* using exactly 150 µg brain mitochondria from 7-wk-old WT and *Parl*$^{-/-}$ mice ($n = 5$ in *C*, $n = 4$ in *D*). (*C*) $\Delta\psi$ using the CI substrates glutamate and malate (GLUT/MAL) without (leak state) and with ADP (phosphorylating state). (*D*) $\Delta\psi$ using the CII substrate succinate in presence of the CI inhibitor rotenone without and with ADP. The graph bars indicate the average ± SD. Statistical significances by two-sided *t* test: $^{**}P < 0.005$ and $^{***}P < 0.0005$.

of ADP was unaltered (Fig. 5 *C* and *D*, *Left*). Therefore, the decreased mitochondrial calcium uptake, which is evaluated in the absence of ADP, is not simply explained by mitochondrial depolarization. In conclusion, PARL deficiency leads to severe alterations of mitochondrial calcium metabolism without overtly inducing oxidative stress in the brain.

Mitochondrial Proteome Changes Induced by PARL Deficiency in the Brain. We wondered what mitochondrial protein changes underlie the observed CIII and CoQ defects in *Parl*$^{-/-}$ brains. We performed an MS-based proteome analysis of brain mitochondria purified from WT and *Parl*$^{-/-}$ mice, leading to the quantification of 781 of 1,085 proteins annotated in the mouse mitochondrial proteome in UniProt (*SI Appendix*, Table S1). The volcano plot showed that, despite the dramatic phenotype, surprisingly few mitochondrial proteins were differentially expressed (Fig. 6*A*), indicating selective effects of PARL on the mitochondrial proteome. Among these, we found a striking down-regulation of the CIII-regulating protein TTC19 (23, 27) and of several proteins required for CoQ biosynthesis (COQ3, COQ4, COQ5). We also noticed a significant decrease of the sulfide-CoQ oxidoreductase SQOR, which has been recently reported to decrease in human primary CoQ defects (28). GHITM, a multipass inner membrane protein not previously linked to PARL, similarly decreased. In contrast, like PINK1 and PGAM5, DIABLO (10) increased in *Parl*$^{-/-}$ brain mitochondria (Fig. 6*A*). Next, we validated these findings by Western blot in brain mitochondria from WT, *Parl*$^{-/-}$, and *Parl*$^{L/L}$::*Nes*^{Cre} mice (Fig. 6*B*). As our proteomic approach identifies substrates by expression changes, we decided to include the previously reported PARL substrates HTRA2 (5), OPA1 (3), STARD7, and CLPB (10) in the validation, despite not being differentially regulated in our MS analysis (Fig. 6*A* and *SI Appendix*, Table S1). Western blots confirmed the virtual disappearance of TTC19; a marked reduction of the CoQ proteins (COQ3, COQ4, COQ5), SQOR, and GHITM; and altered cleavage of TTC19, PGAM5, DIABLO, STARD7, and CLPB. The expression and processing of HTRA2 and OPA1 were not impaired (Fig. 6*B*). To correlate these protein changes with the clinical phenotype, we checked their expression in brain tissue over time, at the ages of 1, 3, and 5 wk, when *Parl*$^{-/-}$ mice are still asymptomatic, and at 7 wk, when the mice are severely affected by neurological deficits (Fig. 6*C* and *SI Appendix*, Fig. S7).

To further investigate the molecular basis of the CIII and CoQ deficiency, we included in this time course an extensive panel of proteins required for CoQ biosynthesis (Fig. 6*C* and *SI Appendix*, Fig. S8). The virtual disappearance of mature TTC19 in *Parl*$^{-/-}$ brains at all ages indicates that PARL is required for TTC19 maturation and expression. COQ4 was also reduced in *Parl*$^{-/-}$ brains already at 1 wk of age, followed by decreased COQ3, COQ5, COQ6, COQ7, COQ9, and SQOR at later time points (Fig. 6*C* and *SI Appendix*, Fig. S8). Other proteins already affected at the age of 1 wk were GHITM and STARD7, in addition to PINK1 and PGAM5, whereas DIABLO accumulated only in late symptomatic stages (*SI Appendix*, Fig. S7). Expression of CLPB, HTRA2, and OPA1 was largely unaffected by PARL expression at all ages, except for a tendency for increased expression of the short Opa1 isoform at 7 wk of age (*SI Appendix*, Fig. S7).

To explore to what extent the catalytic function of PARL is involved in these protein changes, we checked the expression of these proteins in stable *Parl*$^{-/-}$ MEFs expressing PARL^{WT} or catalytic inactive PARL^{S275A} (*SI Appendix*, Fig. S9). We observed no altered mobility of COQ4, COQ5, or SQOR in *Parl*$^{-/-}$ cultured MEFs, suggesting that they likely are not direct PARL substrates. In contrast, the processing of TTC19, PINK1, PGAM5, STARD7, DIABLO, and CLPB was clearly modified by expression of catalytically active PARL, but not by mutant PARL^{S275A}, confirming that PARL proteolytic activity is required for the maturation of these proteins and that they are all likely genuine PARL substrates (10). In contrast, we could again not confirm differences in HTRA2 and OPA1 processing in *Parl*$^{-/-}$ MEFs, suggesting that neither are PARL substrates, in contrast to previous reports (3, 5).

Effect of PARL Deficiency on CIII and CoQ in Liver and Muscle. To investigate to what extent PARL deficiency also affects expression of TTC19 and COQ4 in organs other than the brain, we blotted extracts of liver and skeletal muscle from *Parl*$^{-/-}$, *Parl*$^{L/L}$::*Nes*^{Cre}, and WT mice (*SI Appendix*, Fig. S10 *A* and *B*). As in the nervous system, TTC19 expression was almost absent in liver and skeletal muscle tissue of *Parl*$^{-/-}$ mice only. COQ4 was significantly diminished in both tissues, although to a lesser extent in *Parl*$^{-/-}$ muscle compared with brain and liver. Next, we checked CoQ concentrations and reduced/oxidized (red/ox) ratio as well as CIII activity in muscle and found altered CIII activity and CoQ red/ox

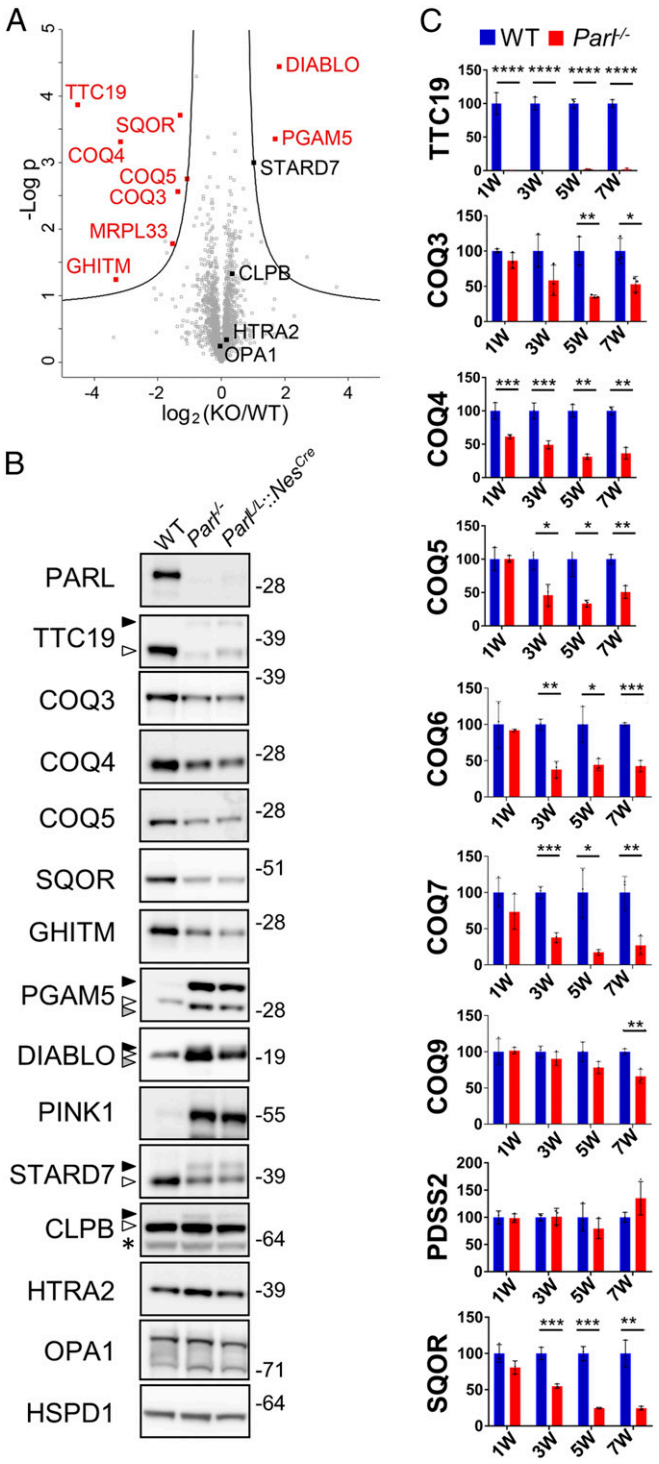

Fig. 6. Restricted changes in the brain mitochondrial proteome induced by PARL deficiency explain the CIII and CoQ defects. (*A*) Volcano plot showing differentially regulated proteins in $Parl^{-/-}$ brain mitochondria purified from 5-wk-old WT and $Parl^{-/-}$ brains ($n = 3$) analyzed by MS. Significantly differentially regulated proteins are distributed outside the volcano cutoff of fold change >2 and *P* value <0.05. Differentially expressed mitochondrial proteins are plotted in red. Previously reported PARL substrates that did not reach statistical significance are plotted in black. The nonmitochondrial proteins TRABD, BCAP31, BCAN, EIF1A, and SETDB were not included in the graph because they appeared unchanged in the validation experiment in *B*. (*B*) Validation of the MS results and of previously reported PARL substrates PINK1, STARD7, CLPB, HTRA2, and OPA1. Brain mitochondria isolated from WT, $Parl^{-/-}$, and $Parl^{L/L}$::Nes^{Cre} were analyzed by immunoblotting. White arrows indicate the mature (processed) form of the protein, black arrows indicate unprocessed forms, and gray arrows indicate alternatively processed forms in $Parl^{-/-}$ mitochondria. The asterisk indicates bands of uncertain significance. (*C*) Time course of TTC19, CoQ biosynthesis proteins, and SQOR in WT and $Parl^{-/-}$ brains. Total brain lysates from WT and $Parl^{-/-}$ mice killed at 1, 3, 5, and 7 wk of age ($n = 3$) were analyzed by immunoblotting (original blots in *SI Appendix*, Fig. S8). The graph bars indicate the quantifications. Each protein was normalized with the loading control HSPD1 and expressed as percentage relative to the WT. The graph bars indicate the average ± SD. Statistical significances by two-sided *t* test: $*P < 0.05$, $**P < 0.01$, $***P < 0.001$, and $****P < 0.0001$.

ratio in $Parl^{-/-}$ muscles but normal CoQ concentration (*SI Appendix*, Fig. S10*C*). These data indicate that PARL is required for the expression of TTC19 and COQ4 in different organs in vivo, although PARL deficiency in muscle compromises only CIII activity and not CoQ concentration.

TTC19 Deficiency Causes CIII Defects and Altered CoQ Red/Ox but Not Altered CoQ Biosynthesis. To dissect the relationship between the TTC19 deficiency and the observed CoQ defects, we generated $Ttc19^{-/-}$ mice (Fig. 7 *A* and *B*). None of these mice ($N = 20$) have shown reduced survival, but they displayed a slight reduction in locomotor activity at 1 y of age. Neuropathological analysis of the brainstem of $Ttc19^{-/-}$ mice at the age of 7 wk did not demonstrate lesions (*SI Appendix*, Fig. S11), as opposed to $Parl^{-/-}$ mice. Blue native gel electrophoresis of $Ttc19^{-/-}$ brain mitochondria showed a similar upward mobility shift of $CIII_2$ as seen with $Parl^{-/-}$ mitochondria (Fig. 7*C*). COQ4 expression (Fig. 7*B*) and CoQ concentration (Fig. 7*D*) were normal, but the CoQ red/ox ratio was highly increased in $Ttc19^{-/-}$ (Fig. 7*E*) as in $Parl^{-/-}$ brains (Fig. 4*H*). Thus, deficiency of mature TTC19 in $Parl^{-/-}$ brains explains the altered CIII structure and function, but not the CoQ biosynthesis deficit. Altogether, the data indicate that PARL is required for the maintenance of CIII activity by stabilization of TTC19 and for efficient CoQ biosynthesis in the brain by stabilization of COQ4 expression (*SI Appendix*, Fig. S12 *A* and *B*).

Discussion

This work reveals an essential role of PARL in the homeostasis of the nervous system. Deficient PARL in the nervous tissue, whether isolated or in the context of systemic *Parl* KO, leads to severe neurodegeneration similar to the CI-deficient $Ndufs4^{-/-}$ mouse (29, 30), the only currently available mouse model for Leigh syndrome. Although caution is needed before extrapolating from mouse to human diseases, the present study prompts an investigation of whether *PARL* gene mutations are present in patients with unexplained Leigh and Leigh-like syndromes. Deletion of *Parl* in the nervous system alone in $Parl^{L/L}$::Nes^{Cre} largely mimics the germline $Parl^{-/-}$ phenotype, like $Ndufs4^{L/L}$::Nes^{Cre} recapitulates that of germline $Ndufs4^{-/-}$ indicating that, in both models, the nervous system involvement drives the disease. This observation demonstrates that the Leigh syndrome is the elusive cause of the multisystem lethal phenotype previously described in $Parl^{-/-}$ mice (3). Interestingly, severe neurological alterations have also been observed in flies carrying mutations in rhomboid-7 (31), the fly ortholog of PARL. Therefore, specific deletion of *Parl* in the nervous system also causes severe atrophy of skeletal muscle, thymus, and spleen as in germline $Parl^{-/-}$ mice (3), although with a delay of approximately 1 month. Nonspecific Cre recombinase activity driven by Nestin was very limited in these tissues, and PARL protein expression was unaffected; it therefore very unlikely contributes to these $Parl^{L/L}$::Nes^{Cre} phenotypes. Moreover, the lack of obvious muscle atrophy and lethality in mice with specific deletion of *Parl* in muscle, as opposed to the nervous system, indicates that the severe muscle atrophy is

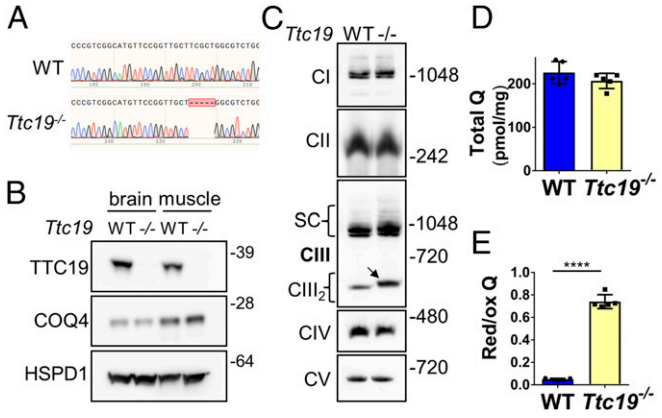

Fig. 7. TTC19 deficiency causes alterations in CIII and CoQ red/ox but not in CoQ concentration in the nervous system. (*A*) Generation of *Ttc19*$^{-/-}$ mice by CRISPR/Cas9 technology. *Ttc19*$^{-/-}$ mice have a 5-bp deletion in the first exon. (*B*) Immunoblot analysis of brain and muscle mitochondria with anti-TTC19 and COQ4 antibodies. HSPD1 is the loading control. (*C*) Blue native gel electrophoresis of purified brain mitochondria from 7-wk-old WT and *Ttc19*$^{-/-}$ mice, followed by immunoblotting with anti-NDUFS3 (CI), anti-SDHA (CII), anti-UQCRFS1 (CIII), anti-COX4I1 (CIV), and anti-ATP5B (CV). The arrow indicates the upward mobility change of $CIII_2$ in *Ttc19*$^{-/-}$ mitochondria. (*D*) Concentration of total CoQ (Q_9+Q_{10}) in brains from 7-wk-old WT and *Ttc19*$^{-/-}$ mice ($n = 5$). (*E*) CoQ red/ox ratio from the experiment in *D*. Bar graphs indicate average ± SD. Statistical significance calculated by two-sided Student *t* test: ****$P < 0.0001$.

mainly a consequence of the neurodegeneration. Brain-specific deletion of the mitochondrial protease HTRA2 affects thymus and spleen in a similar way as brain-specific PARL deficiency (32). Such immunological phenotypes can be caused by a variety of general stress conditions that trigger increased secretion of corticosteroids and other stress hormones, which induce apoptosis in these tissues (33). Hindlimb unloading, for instance (34), induces the distinctive depletion of double-positive $CD4^+$ $CD8^+$ T lymphocytes that was also observed in *Parl*$^{-/-}$ thymus and a decrease of B lymphocytes as seen in *Parl*$^{-/-}$ spleen (3), but general stress conditions such as malnutrition (35) or neurological diseases (36) can have similar effects on apoptosis in thymus and spleen, at least in mice. This is consistent with the observation that *Parl*$^{-/-}$ and *Parl*$^{L/L}$::*Nes*^{Cre} mice develop these immunological manifestations only in late stages of the neurological disease.

Since the original description of *Parl*$^{-/-}$ mice (3), many studies have focused on possible links between PARL and apoptosis in vitro, with controversial results (3, 5, 10). Here we were unable to confirm a role of PARL in apoptosis in vivo (3) and instead observed a severe necrotic neuronal phenotype. We speculate that the necrotic encephalopathy may represent a tissue-specific consequence of the severe structural and functional damage that progressively accumulates in *Parl*$^{-/-}$ neuronal mitochondria, rather than the result of a direct gatekeeping activity of PARL in regulated necrosis machineries. Although we were not able to define in further detail whether necrosis is regulated in *Parl*$^{-/-}$ brains, the neuropathological phenotype is consistent with the definition of Leigh syndrome as a necrotizing encephalomyelopathy.

Surprisingly, despite the striking neuropathology, the absence of PARL affects only a very circumscribed proportion of the brain mitochondrial proteome, which overlaps with recent proteomic data obtained in HEK293 cells (10). One limitation of our proteomic approach is that it evaluated only protein expression and not posttranslational modifications, and, in particular, cleavage sites were not analyzed. At odds with previous observations (3, 5) and consistent with more recent reports (10, 37), the data presented here do not support OPA1 and HTRA2 as substrates of PARL. Conversely, we find several proteins differentially regulated by PARL deficiency, and several of them play important roles in neurological diseases. We tested explicitly whether PINK1 and PGAM5, two substrates of PARL involved in Parkinson's disease (11, 12) and mitophagy (12, 21), could drive the pathological phenotype of *Parl*$^{-/-}$ mice. Rare *PARL* mutations have been reported in patients with Parkinson's disease (16). We tested combined KOs of these two substrates with *Parl*$^{-/-}$ and their combined deletion in the presence of PARL to check whether the accumulation or the loss of function of these two substrates would play a role, but none of these experiments modulated or simulated the *Parl*$^{-/-}$ phenotype. Thus, PINK1 and PGAM5 are not responsible for the Leigh-like pathology in the *Parl*$^{-/-}$ mice, indicating that other biochemical mechanisms are involved.

Here we show that PARL plays an essential role in the respiratory chain independently from effects on mitochondrial mass (14) by regulating proteins implicated in CIII and CoQ biogenesis. PARL is required for the expression of TTC19 (Fig. 6 *B* and *C*), and impaired proteolytic maturation of TTC19 by PARL likely leads to its degradation by alternative mitochondrial proteases. A recent study reported that PARL is required for TTC19 cleavage in vitro (10), but the functional consequences were not investigated. TTC19 is involved in the turnover of the iron-sulfur protein UQCRFS1 (23), a structural subunit of CIII essential for the catalytic activity that ensures CoQ oxidation. Here we show that impaired proteolytic maturation and expression of TTC19 in *Parl*$^{-/-}$ tissues results in altered CIII structure and catalytic activity, as in *Ttc19*$^{-/-}$ mitochondria. The defective CIII activity is reflected by the increased fraction of reduced vs. oxidized CoQ. When CIII activity is normal, CoQ red/ox ratio is low, whereas it is high when CIII is dysfunctional, in *Parl*$^{-/-}$ and *Ttc19*$^{-/-}$ mice. In addition, and independently from TTC19, PARL modulates the expression of COQ4, a protein required for the biosynthesis of CoQ (38). Intriguingly, the severe CoQ deficiency we found in *Parl*$^{-/-}$ brains is followed by a secondary reduction in the expression of SQOR, as also recently observed in primary CoQ defects (28). CoQ is a highly hydrophobic molecule functioning as an electron carrier from several metabolic pathways to CIII and as membrane antioxidant (39, 40). The mechanism that links ablation of PARL to the reduced COQ4 and the resulting CoQ deficiency in the brain is, however, not yet clear, as we could not demonstrate that COQ4 is a substrate of PARL. One possibility is that misprocessing of a still undefined PARL substrate affects CoQ biosynthesis upstream of COQ4, similarly to how the yeast intermediate peptidase Oct1p ensures CoQ biosynthesis by cleaving Coq5p (41). An alternative hypothesis is that PARL regulates CoQ biosynthesis indirectly by generating an early stress response that precedes the respiration defects. Recent observations show that the CoQ pathway is sensitive to different mechanisms affecting mitochondrial DNA gene expression in mouse heart tissue (42). However, in these models, PARL expression was up-regulated, whereas COQ4 was unmodified or increased, in contrast with what we observe in *Parl*$^{-/-}$ mice. Thus, the effects caused by PARL deficiency are clearly different from those reported in that study.

The *Ttc19*$^{-/-}$ mouse data indicate that the CoQ deficiency is independent from the CIII defect, and therefore PARL plays an essential role in the maintenance of the respiratory chain by two distinct mechanisms. Interestingly, human mutations in *TTC19* (24) and in genes that induce CoQ deficiency (19) are independent causes of Leigh syndrome. In addition, *COQ4* haploinsufficiency causes neurodegeneration in humans (38). However, deletion of *Ttc19* in mouse causes only mild neurodegeneration at advanced ages (23), and, accordingly, we did not observe in *Ttc19*$^{-/-}$ mice the massive brainstem encephalopathy of *Parl*$^{-/-}$ mice at comparable age (*SI Appendix*, Fig. S11). One hypothesis is that the respiratory chain dysfunction determined by the combination of the CIII and CoQ defects drive the *Parl*$^{-/-}$ Leigh-like encephalopathy. This might be a possible explanation

for the apparent resistance of the skeletal muscle to *Parl* ablation, as, in this tissue, decreased COQ4 was not associated with a significant decrease in CoQ concentration, as in the brain. However, we cannot exclude that other mitochondrial functional and structural defects caused by PARL deficiency could also contribute to the pathogenesis of the neurodegeneration. We did not find a major impact of PARL deficiency in oxidative stress in the brain, but we found severe consequences on mitochondrial calcium metabolism. Mitochondrial calcium is a critical determinant of cell death, including necrosis, and is particularly important in many neurodegenerative disorders, including Parkinson's disease, amyotrophic lateral sclerosis, Huntington disease (26), and hereditary neurological diseases caused by mutations in another mitochondrial protease, *AFG3L2* (43). Moreover, mitochondrial function and structure are bidirectionally related, and we found that $Parl^{-/-}$ brain mitochondria progressively accumulate morphological abnormalities, implying that PARL plays a role, whether direct or indirect, in mitochondrial ultrastructure. It is thus plausible that the drastic neurodegeneration that we report in $Parl^{-/-}$ mice is the result of a combination of mitochondrial functional and structural defects that progressively accumulate, culminating in neuronal necrosis.

Our work indicates that PARL has a constitutive physiological role in keeping mitochondrial function and structural integrity in check, with crucial consequences for the nervous system.

Materials and Methods

Details of study materials and methods are provided in *SI Appendix, Material and Methods*, including details on mice, pathology, in situ hybridization, EM, subcellular fractionation, immunoblots, blue native gel electrophoresis, high-resolution respirometry, mitochondrial respiratory chain enzyme CoQ, ROS production, protein carbonylation, mitochondrial calcium, mitochondrial potential antibodies, proteomics, plasmids, mtDNA quantifications, cell culture, and statistics. All experiments were approved by the Ethical Committee on Animal Experimentation of the University of Leuven (KU Leuven).

ACKNOWLEDGMENTS. We thank A. Francis, E. Seuntjens, V. Hendrickx, and J. Verwaeren for help. This work was supported by Fonds voor Wetenschappelijk Onderzoek, a Methusalem Grant, Geneeskundige Stichting Koningin Elisabeth, Bax-Vanluffelen, "Opening the Future," Vlaams Initiatief voor Netwerken voor Dementie Onderzoek, the Spanish Ministry of Health (Grant PI17-01286), and Hercules Grant AKUL/09/037. M.S. is a recipient of European Molecular Biology Organization long-term fellowship ALTF 648-2013.

1. Spinazzi M, De Strooper B (2016) PARL: The mitochondrial rhomboid protease. *Semin Cell Dev Biol* 60:19–28.
2. Düsterhöft S, Künzel U, Freeman M (2017) Rhomboid proteases in human disease: Mechanisms and future prospects. *Biochim Biophys Acta Mol Cell Res* 1864: 2200–2209.
3. Cipolat S, et al. (2006) Mitochondrial rhomboid PARL regulates cytochrome c release during apoptosis via OPA1-dependent cristae remodeling. *Cell* 126:163–175.
4. Anand R, et al. (2014) The i-AAA protease YME1L and OMA1 cleave OPA1 to balance mitochondrial fusion and fission. *J Cell Biol* 204:919–929.
5. Chao J-R, et al. (2008) Hax1-mediated processing of HtrA2 by Parl allows survival of lymphocytes and neurons. *Nature* 452:98–102.
6. Deas E, et al. (2011) PINK1 cleavage at position A103 by the mitochondrial protease PARL. *Hum Mol Genet* 20:867–879.
7. Jin SM, et al. (2010) Mitochondrial membrane potential regulates PINK1 import and proteolytic destabilization by PARL. *J Cell Biol* 191:933–942.
8. Meissner C, Lorenz H, Weihofen A, Selkoe DJ, Lemberg MK (2011) The mitochondrial intramembrane protease PARL cleaves human Pink1 to regulate Pink1 trafficking. *J Neurochem* 117:856–867.
9. Sekine S, et al. (2012) Rhomboid protease PARL mediates the mitochondrial membrane potential loss-induced cleavage of PGAM5. *J Biol Chem* 287:34635–34645.
10. Saita S, et al. (2017) PARL mediates Smac proteolytic maturation in mitochondria to promote apoptosis. *Nat Cell Biol* 19:318–328.
11. Valente EM, et al. (2004) Hereditary early-onset Parkinson's disease caused by mutations in PINK1. *Science* 304:1158–1161.
12. Lu W, et al. (2014) Genetic deficiency of the mitochondrial protein PGAM5 causes a Parkinson's-like movement disorder. *Nat Commun* 5:4930.
13. Greene AW, et al. (2012) Mitochondrial processing peptidase regulates PINK1 processing, import and Parkin recruitment. *EMBO Rep* 13:378–385.
14. Civitarese AE, et al. (2010) Regulation of skeletal muscle oxidative capacity and insulin signaling by the mitochondrial rhomboid protease PARL. *Cell Metab* 11:412–426.
15. Jeyaraju DV, et al. (2006) Phosphorylation and cleavage of presenilin-associated rhomboid-like protein (PARL) promotes changes in mitochondrial morphology. *Proc Natl Acad Sci USA* 103:18562–18567.
16. Shi G, et al. (2011) Functional alteration of PARL contributes to mitochondrial dysregulation in Parkinson's disease. *Hum Mol Genet* 20:1966–1974.
17. Meissner C, Lorenz H, Hehn B, Lemberg MK (2015) Intramembrane protease PARL defines a negative regulator of PINK1- and PARK2/Parkin-dependent mitophagy. *Autophagy* 11:1484–1498.
18. Shi G, McQuibban GA (2017) The mitochondrial rhomboid protease PARL is regulated by PDK2 to integrate mitochondrial quality control and metabolism. *Cell Rep* 18: 1458–1472.
19. Lake NJ, Compton AG, Rahman S, Thorburn DR (2016) Leigh syndrome: One disorder, more than 75 monogenic causes. *Ann Neurol* 79:190–203.
20. Lake NJ, Bird MJ, Isohanni P, Paetau A (2015) Leigh syndrome: Neuropathology and pathogenesis. *J Neuropathol Exp Neurol* 74:482–492.
21. Yamano K, Youle RJ (2013) PINK1 is degraded through the N-end rule pathway. *Autophagy* 9:1758–1769.
22. Wang Z, Jiang H, Chen S, Du F, Wang X (2012) The mitochondrial phosphatase PGAM5 functions at the convergence point of multiple necrotic death pathways. *Cell* 148:228–243.
23. Bottani E, et al. (2017) TTC19 plays a husbandry role on UQCRFS1 turnover in the biogenesis of mitochondrial respiratory complex III. *Mol Cell* 67:96–105.e4.
24. Koch J, et al. (2015) Mutations in TTC19: Expanding the molecular, clinical and biochemical phenotype. *Orphanet J Rare Dis* 10:40.
25. Guarás A, et al. (2016) The CoQH2/CoQ ratio serves as a sensor of respiratory chain efficiency. *Cell Rep* 15:197–209.
26. Abeti R, Abramov AY (2015) Mitochondrial $Ca^{(2+)}$ in neurodegenerative disorders. *Pharmacol Res* 99:377–381.
27. Ghezzi D, et al. (2011) Mutations in TTC19 cause mitochondrial complex III deficiency and neurological impairment in humans and flies. *Nat Genet* 43:259–263.
28. Ziosi M, et al. (2017) Coenzyme Q deficiency causes impairment of the sulfide oxidation pathway. *EMBO Mol Med* 9:96–111.
29. Kruse SE, et al. (2008) Mice with mitochondrial complex I deficiency develop a fatal encephalomyopathy. *Cell Metab* 7:312–320.
30. Quintana A, Kruse SE, Kapur RP, Sanz E, Palmiter RD (2010) Complex I deficiency due to loss of Ndufs4 in the brain results in progressive encephalopathy resembling Leigh syndrome. *Proc Natl Acad Sci USA* 107:10996–11001.
31. McQuibban GA, Lee JR, Zheng L, Juusola M, Freeman M (2006) Normal mitochondrial dynamics requires rhomboid-7 and affects Drosophila lifespan and neuronal function. *Curr Biol* 16:982–989.
32. Patterson VL, et al. (2014) Neural-specific deletion of Htra2 causes cerebellar neurodegeneration and defective processing of mitochondrial OPA1. *PLoS One* 9:e115789.
33. Dooley J, Liston A (2012) Molecular control over thymic involution: From cytokines and microRNA to aging and adipose tissue. *Eur J Immunol* 42:1073–1079.
34. Wang KX, Shi Y, Denhardt DT (2007) Osteopontin regulates hindlimb-unloading-induced lymphoid organ atrophy and weight loss by modulating corticosteroid production. *Proc Natl Acad Sci USA* 104:14777–14782.
35. Savino W (2002) The thymus gland is a target in malnutrition. *Eur J Clin Nutr* 56(suppl 3):S46–S49.
36. Seksenyan A, et al. (2010) Thymic involution, a co-morbidity factor in amyotrophic lateral sclerosis. *J Cell Mol Med* 14:2470–2482.
37. Jeyaraju DV, Cisbani G, De Brito OM, Koonin EV, Pellegrini L (2009) Hax1 lacks BH modules and is peripherally associated to heavy membranes: Implications for Omi/HtrA2 and PARL activity in the regulation of mitochondrial stress and apoptosis. *Cell Death Differ* 16:1622–1629.
38. Salviati L, et al. (2012) Haploinsufficiency of COQ4 causes coenzyme Q10 deficiency. *J Med Genet* 49:187–191.
39. Alcázar-Fabra M, Navas P, Brea-Calvo G (2016) Coenzyme Q biosynthesis and its role in the respiratory chain structure. *Biochim Biophys Acta* 1857:1073–1078.
40. Stefely JA, Pagliarini DJ (2017) Biochemistry of mitochondrial coenzyme Q biosynthesis. *Trends Biochem Sci* 42:824–843.
41. Veling MT, et al. (2017) Multi-omic mitoprotease profiling defines a role for Oct1p in coenzyme Q roduction. *Mol Cell* 68:970–977.e11.
42. Kühl I, et al. (2017) Transcriptomic and proteomic landscape of mitochondrial dysfunction reveals secondary coenzyme Q deficiency in mammals. *eLife* 6:e30952.
43. Maltecca F, et al. (2015) Purkinje neuron Ca2+ influx reduction rescues ataxia in SCA28 model. *J Clin Invest* 125:263–274.